Density of states for random-central-force elastic networks

E. J. Garboczi* and M. F. Thorpe
Department of Physics and Astronomy, Michigan State University, East Lansing, Michigan 48824-1116
(Received 19 February 1985)

Effective-medium theory (EMT) results for the behavior of the elastic properties of random-central-force networks with a fraction p of nearest-neighbor bonds present are extended to *finite frequencies*. Good agreement with numerical simulations for the density of states at all frequencies is demonstrated. In particular, the gap at $\omega^2=0$ that opens up when $p=p^*$, and the loss of elastic properties are correctly predicted. The fraction of zero-frequency modes is well described by the EMT and by constraint counting which leads to the same result. The only substantial error is that the EMT does *not* give Lifshitz tails at the band edges.

I. INTRODUCTION

Recently it was shown that a simple effective-medium theory (EMT) gives an excellent description of the elastic properties of central-force elastic networks created by randomly removing nearest-neighbor central-force bonds from a Bravais lattice.[1] The elastic moduli of model networks were computed via numerical simulation as a function of p (the fraction of bonds present) and were shown to go to zero at the rigidity threshold p^*, whose value was found to be very near $2d/z$ (where d is the dimensionality and z is the nearest-neighbor coordination in the pure system), a result previously obtained by constraint counting.[2] The value of p^* is much higher than p_c, the critical threshold for ordinary connectivity percolation, since these networks contain units which are fully connected but cannot resist an external strain, and so belong to a new category of problem called *rigidity percolation*.[1-3] In this paper we present the first results for the finite-frequency response of a system undergoing a rigidity transition.

The EMT was derived in two independent ways:[1] The *static method* is an adaptation of an EMT developed by Kirkpatrick[4] for the conduction problem, and the second method is based on the coherent-potential approximation (CPA).[5] Only the elastic behavior of the networks was addressed in Ref. 1; however, the CPA-based EMT can easily be extended to give a prediction for the density of states of the network at all frequencies, as is shown in Sec. III. The static method can also be extended to finite frequencies and gives identical results. This paper reports on the finite-frequency results for the central-force elastic networks, thus completing the description begun in Ref. 1 and shows that the EMT gives a reasonable description of the finite-frequency properties, although it fails to describe the Lifshitz tails and structure due to small clusters as would be expected. Some of the qualitative effects of the rigidity transition at $p=p^*$ on the density of states are demonstrated well by both numerical simulation and EMT.

All the results in this paper are for the triangular net with nearest-neighbor central forces. Similar results would be expected for other stable lattices like fcc. In Sec. IV we describe the numerical simulations and compare them with the EMT results. Section V presents our conclusions and makes comparisons with results on other systems.

II. PURE SYSTEM

Two models were studied in Ref. 1: the triangular net and the fcc lattice. In this work we focus on the triangular net. It is important to understand the pure-system density of states (DOS) before one can see how the DOS evolves as bonds are cut.

The lattice potential used is central and harmonic:

$$V=\frac{\alpha}{2}\sum_{\langle i,j\rangle}[(\mathbf{u}_i-\mathbf{u}_j)\cdot\hat{\mathbf{r}}_{ij}]^2 p_{ij}\ , \tag{1}$$

where $\hat{\mathbf{r}}_{ij}$ is a unit vector from site i to site j, $\mathbf{u}_i$ is the displacement from equilibrium of the particle with mass M at site i, p_{ij} is 0,1 respectively, as the bond between i and j is missing or present, α is the spring force constant, and $\langle i,j\rangle$ under the summation means that i and j are nearest neighbors, and each pair is counted just once. One can construct the 2×2 dynamical matrix[6] $\overleftrightarrow{D}(\mathbf{k})$ from V with the result

$$\overleftrightarrow{D}(\mathbf{k})=\begin{bmatrix} \frac{\alpha}{M}\left[3-2\cos(k_x a)-\cos(\tfrac{1}{2}k_x a)\cos\left[\frac{\sqrt{3}}{2}k_y a\right]\right], & \frac{\sqrt{3}\alpha}{M}\sin(\tfrac{1}{2}k_x a)\sin\left[\frac{\sqrt{3}}{2}k_y a\right] \\ \frac{\sqrt{3}\alpha}{M}\sin(\tfrac{1}{2}k_x a)\sin\left[\frac{\sqrt{3}}{2}k_y a\right], & \frac{3\alpha}{M}\left[1-\cos(\tfrac{1}{2}k_x a)\cos\left[\frac{\sqrt{3}}{2}k_y a\right]\right] \end{bmatrix}. \tag{2}$$

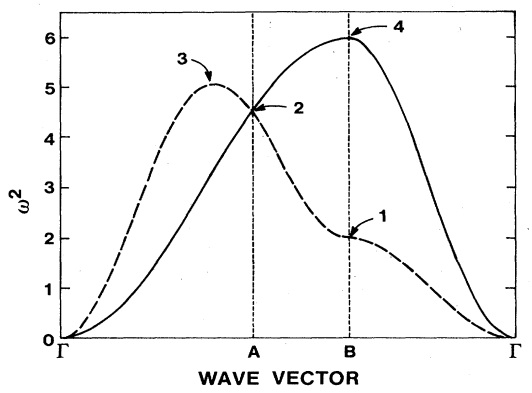

FIG. 1. Dispersion relation $\omega^2(\mathbf{k})$ for the triangular net with lattice potential (1) plotted along the pathway Γ-A-B-Γ in the first Brillouin zone shown in Fig. 2. The abscissa is in units where $\alpha/M=1$ [see Eqs. (3)]. The special points labeled 1—4 are also shown in Fig. 3.

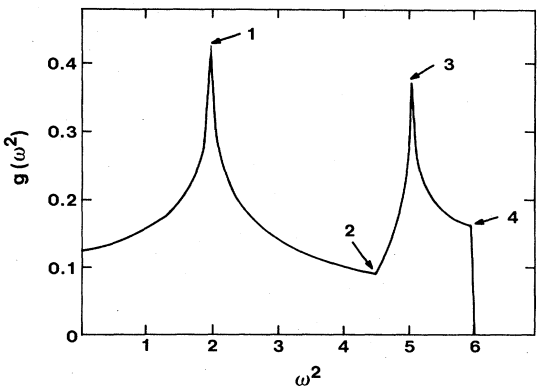

FIG. 3. Vibrational density of states $g(\omega^2)$ for the pure triangular net. The units are such that $\alpha/M=1$, which puts the maximum frequency at $\omega^2=6$. The special points labeled 1—4 are also shown in Fig. 1.

Diagonalizing $\overleftrightarrow{D}(\mathbf{k})$, we obtain the phonon dispersion relations $\omega^2(\mathbf{k})$, given by

$$\omega^2(\mathbf{k})=\frac{\alpha}{M}[W_1\pm(W_2)^{1/2}]\,,$$

$$W_1=3-\cos(k_xa)-2\cos(\tfrac{1}{2}k_xa)\cos\left[\frac{\sqrt{3}}{2}k_ya\right]\,, \tag{3}$$

$$W_2=\left[\cos(\tfrac{1}{2}k_xa)\cos\left[\frac{\sqrt{3}}{2}k_ya\right]-\cos(k_xa)\right]^2 +3\sin^2(\tfrac{1}{2}k_xa)\sin^2\left[\frac{\sqrt{3}}{2}k_ya\right]\,,$$

where a is the nearest-neighbor bond length. Figure 1 shows the two branches of $\omega^2(\mathbf{k})$ plotted along the pathway Γ-A-B-Γ (see Fig. 2) in the first Brillouin zone of the triangular net.

Knowing $\omega^2(\mathbf{k})$, we can easily generate the DOS $g(\omega^2)$ by randomly selecting points in $\mathbf{k}$ space and counting the number of points falling in any given small range of ω^2. Figure 3 shows the result for the pure-system DOS obtained in this way. There are critical points at $M\omega^2/\alpha=2$, 4.5, 5, and 6 resulting from local extrema in $\omega^2(\mathbf{k})$. As bonds are randomly removed and p decreases from 1, the DOS will be seen to evolve from the form shown in Fig. 3.

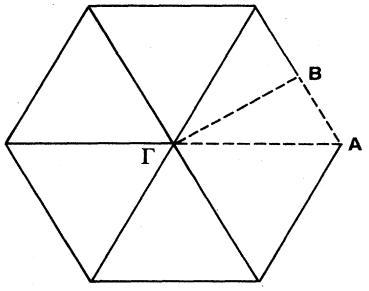

FIG. 2. First Brillouin zone of the triangular net, showing the symmetry points Γ, A, and B.

III. EFFECTIVE-MEDIUM THEORY

The derivation of the CPA-based EMT was given in Ref. 1. Equations (27) and (28) from that work are reproduced here as Eqs. (4) and (5):

$$\left\langle\frac{\alpha-\alpha_m}{1-2(\alpha-\alpha_m)\hat{\mathbf{r}}_{12}\cdot(\overleftrightarrow{P}_{11}-\overleftrightarrow{P}_{12})\cdot\hat{\mathbf{r}}_{12}}\right\rangle=0\,, \tag{4}$$

$$M\omega^2P_{11}=1+\frac{z\alpha_m}{d}\hat{\mathbf{r}}_{12}\cdot(\overleftrightarrow{P}_{11}-\overleftrightarrow{P}_{12})\cdot\hat{\mathbf{r}}_{12}\,, \tag{5}$$

where $\overleftrightarrow{P}_{11},\overleftrightarrow{P}_{12}$ are the diagonal and nearest-neighbor effective-medium Green's functions, respectively, α_m is the effective-medium force constant (complex and energy dependent in general), and $p^*=2d/z$ is the EMT rigidity threshold. Equation (4) is the basic EMT result derived in Ref. 1, and Eq. (5) is the equation of motion for the isotropic site-diagonal Green's function. Using Eq. (5) to simplify Eq. (4), we obtain the CPA equation whose solutions are described in Sec. IV:

$$\alpha[p+p^*(M\omega^2P_{11}-1)]-\alpha_m[1+p^*(M\omega^2P_{11}-1)]=0\,. \tag{6}$$

P_{11} and α_m are complex, in general, so that Eq. (6) can be thought of as a pair of coupled equations for the real (α_m^R) and imaginary (α_m^I) parts of α_m. $P_{11}(\omega^2,\alpha_m)$ is defined as

$$P_{11}(\omega^2,\alpha_m)=\frac{1}{2NM}\sum_{\mathbf{k},s}\frac{1}{\omega^2-\omega_s^2(\mathbf{k})}\,, \tag{7}$$

where the sums are over the first Brillouin zone and the two branches ($s=1,2$) of the dispersion relations shown in Fig. 1 [with α replaced by α_m in Eq. (3)]. The EMT DOS $g_{\text{eff}}(\omega^2)$ can be calculated from

$$g_{\text{eff}}(\omega^2) = -\frac{M}{\pi}\text{Im}P_{11}(\omega^2,\alpha_m) , \quad (8)$$

so that the weight under $g_{\text{eff}}(\omega^2)$ is normalized to 1.

Equation (6) can be solved by iteration for all values of ω^2 (except for a few cases discussed later). One computes P_{11} via numerical integration for an initial value of α_m, and then the new value of α_m is computed via Eq. (6). This process is iterated until the values of α_m and P_{11} converge to within about a percent. Typically this required 6–12 iterations. The last values of P_{11} and α_m are saved, and $g_{\text{eff}}(\omega^2)$ is extracted from $\text{Im}P_{11}$.

IV. RESULTS

The numerical simulation results for the DOS, which is the "experimental" data with which we compare $g_{\text{eff}}(\omega^2)$ were generated using the standard negative eigenvalue method (NEM)[7,8] but adapted for use with sparse random matrices, so that only the nonzero matrix elements are stored and processed. The model networks studied with the NEM were the same three configurations of the triangular networks used in Ref. 1 which had 440 sites (20×22) and periodic boundary conditions. The NEM computes the *number* of modes with eigenvalues less than zero for the matrix $\overleftrightarrow{A}=\overleftrightarrow{D}-\omega^2\overleftrightarrow{I}$, where $\overleftrightarrow{D}$ is the real-space dynamical matrix for the network,[1] and thus the number of modes with frequencies less than ω^2. The NEM leads to the DOS $g(\omega^2)$ in histogram form. The accuracy of the histogram is limited only by finite-size noise and the bin sizes chosen. The essential parameter for the finite-size noise is the average number of modes per bin, which depends on *both* the system size and the bin size. For all the work reported on in this paper, typically 20 bins were used so that there were about 132 modes per bin on the average [a total of three configurations were used to average $g(\omega^2)$]. To get significantly higher resolution in the NEM histograms, we would have to use much larger systems. For the purposes of this study, the systems used were of adequate size.

Four values of p were selected at which to compare the CPA and NEM results. They were (1) $p=0.85$, (2) $p=0.70$, (3) $p=0.50$, and (4) $p=0.20$. The first value was chosen to be close to the crystal and well out of the critical region, where the CPA might be expected to be quite accurate. Point (2) was chosen to be just above $p^*=2d/z=\frac{2}{3}$ ($d=2$, $z=6$) in order to provide a stringent test of the accuracy of the CPA close to the critical region. The value of $p=0.50$ was chosen because when 50% of the bonds are present, the triangular network is still connected geometrically but disconnected elastically, i.e., all moduli are zero.[9] Finally, at $p=0.20$, the network consists only of isolated clusters, since

$$p_c = 2\sin(\pi/18) = 0.3743$$

for the triangular net.[10]

Figure 4 shows the results for the DOS at $p=0.85$. The dashed line is the CPA result $g_{\text{eff}}(\omega^2)$ while the histogram is the NEM experimental determination of $g(\omega^2)$. At the level of accuracy of the histogram the agreement between NEM and CPA is good. One can see the memory of the crystal in the broad peaks which remain at $M\omega^2/\alpha=2$ and 5, while the effect of bond cutting shows in the increase in the low-frequency density of states, since

$$g(\omega^2) = \left[\frac{M}{8\pi}\right](C_{11}^{-1}+C_{44}^{-1}) \sim (p-p^*)^{-1} \text{ as } \omega^2\to 0$$

(see Ref. 11). All these features including the decrease of the right band edge are reproduced well by the CPA. The integrated weight under $g_{\text{eff}}(\omega^2)$ is equal to 1, as it should be.

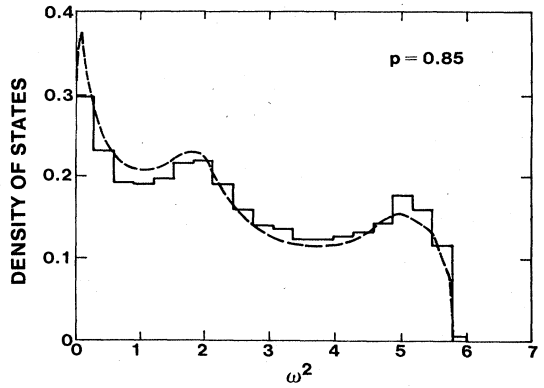

FIG. 4. Density-of-states histogram for the $p=0.85$ networks, averaged over three configurations. The dashed line is the effective-medium result discussed in the text and $\alpha/M=1$.

The DOS results for $p=0.70$ are shown in Fig. 5. The agreement between CPA and NEM is similar to that in Fig. 4. The CPA has a very narrow peak at small ω^2 that goes up off the graph to about 1.9 and then comes back down to the correct $\omega^2=0$ result (which can be obtained from the elastic constants[1]). The bin size used in the histogram was not small enough to check if this behavior was real or an artifact of the CPA. Our networks were not big enough to justify smaller bin sizes because of the noise problem mentioned above. One can clearly see in Fig. 5 the beginning of the divergence of $g(0)$ as the elastic moduli go to zero with $p\to p^*$. The right band edge of

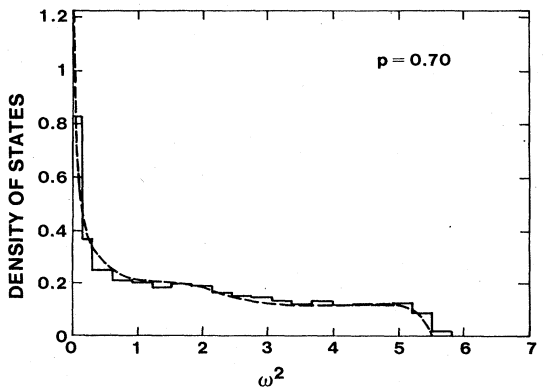

FIG. 5. Density-of-states histogram for the $p=0.70$ networks averaged over three configurations. The dashed line is the effective-medium result, and $\alpha/M=1$.

$g(\omega^2)$ continues to decrease as p decreases, with the CPA roughly tracking this behavior.

At $p=0.50$, the network is connected geometrically but disconnected elastically. Figure 6 presents the CPA and NEM results for this value of p. Again, the overall shape of $g(\omega^2)$ is reproduced by $g_{\text{eff}}(\omega^2)$ to the level of accuracy of the histogram. The one systematic deviation is at the right band edge where the CPA cuts off before the actual band edge. The CPA shows a small gap opening up at low frequencies, with the new band edge at about $M\omega^2/\alpha \approx 0.05$. This is to be expected, as the network has *no* acoustic modes for $p < p^*$. The histogram does not have fine enough resolution to see this effect. In reality we would expect Lifshitz tails[12] at both band edges. It is difficult to solve the CPA Eq. (6) in this region since, to get the band gap, the solution to Eq. (6) must jump from the Riemann sheet that was valid above the rigidity transition to a new solution sheet in the gap. At $p=0.50$, the value of f[1,2] (the fraction of modes with zero frequency) should be

$$f(p)=1-p/p^*=0.25 \ . \tag{9}$$

Therefore, the integrated weight in the band should be 0.75, which it is for *both* the NEM and CPA DOS. The contribution to the DOS from the zero frequency modes will be a δ function at the origin with weight 0.25. This is not shown in Fig. 5; however, the CPA *does* give this δ function with the proper weight $f(p)$ given in Eq. (9) as will be shown below.

At $p=0.20$, the network consists of isolated clusters of sites and bonds, with many clusters containing only one or two bonds. This is reflected in the NEM results shown in Fig. 7. The disproportionately large weight in the bins at $M\omega^2/\alpha=1.5$, 2.0, and 2.5 come from one- and two-bond clusters. These are isolated cluster modes, and obviously a simple effective-medium theory cannot be expected to get these right. However, the CPA does not do too badly in reproducing the other features of the density of states. The overall shape of the density of states, excluding the isolated cluster peaks, is reproduced fairly well by the CPA. At $p=0.20$ the weight at zero frequency is 0.7, so

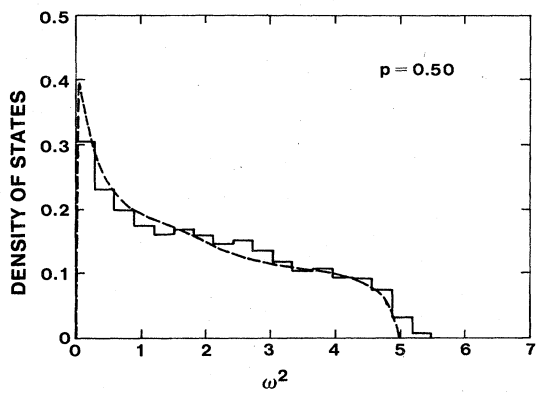

FIG. 6. Density-of-states histogram for the $p=0.50$ networks, averaged over three configurations. The dashed line is the effective-medium result, and $\alpha/M=1$.

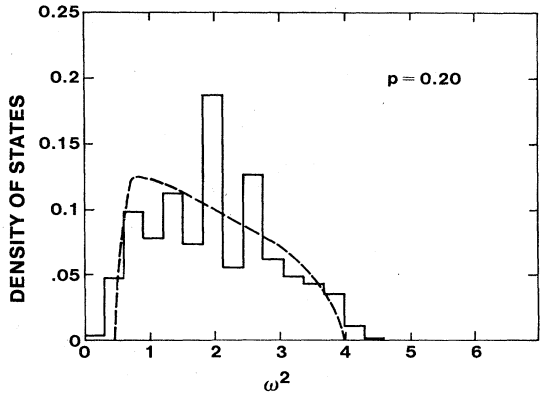

FIG. 7. Density-of-states histogram for the $p=0.20$ networks averaged over three configurations. The dashed line is the effective-medium result, and $\alpha/M=1$.

that the weight in the band is 0.3. The weight under the CPA and NEM curves is equal to this value within computational error.

The CPA in the floppy region below p^* predicts a δ function at the origin with a weight which agrees with the result from constraint counting,[2] $f(p)=1-p/p^*$. This comes about in the following way. Assume that for $p < p^*$, as $\omega^2 \to 0$, α_m^R and $\alpha_m^I \to 0$ as well. Then Eq. (6) can be rearranged to become

$$P_{11}=(1-p/p^*)\frac{1}{\omega^2} \ . \tag{10}$$

When we take the imaginary part of P_{11} to get $g(\omega^2)$, we find that

$$g_{\text{eff}}(\omega^2)=-\frac{M}{\pi}\text{Im}P_{11}=(1-p/p^*)\delta(\omega^2) \ , \tag{11}$$

which agrees with the result from constraint counting. In Fig. 8 the real and imaginary parts of α_m are shown as functions of ω^2 for $p=0.85$ and 0.20. For $p=0.20$ it is clear that *both* α_m^R and α_m^I go to zero with ω^2, so that the CPA does indeed give the result of Eq. (11). The graph of α_m for $p=0.85$ shows the real part going to

$$0.55=\left.\frac{p-p^*}{1-p^*}\right|_{p=0.85} \ , \tag{12}$$

which agrees with the EMT of Ref. 1. One should also note that α_m^I is zero outside the band. This is because the only way $g_{\text{eff}}(\omega^2)$ can be nonzero is if $\text{Im}P_{11}$ is nonzero, and that will occur only when α_m has a finite imaginary part.

Other features of interest in Fig. 8 are the cusplike behaviors of α_m^R ($p=0.20$) for low frequencies. This is an indication that the solution changes sheets in going from in the band to below the band, as was mentioned previously. The solution

$$\alpha_m^R(\omega^2=0)=\alpha(p-p^*)/(1-p^*) \tag{13}$$

remains a solution below p^* as well as above, but below p^* it is not the *physical* solution as it gives elastic behavior at low frequencies. For $p < p^*$ at low frequen-

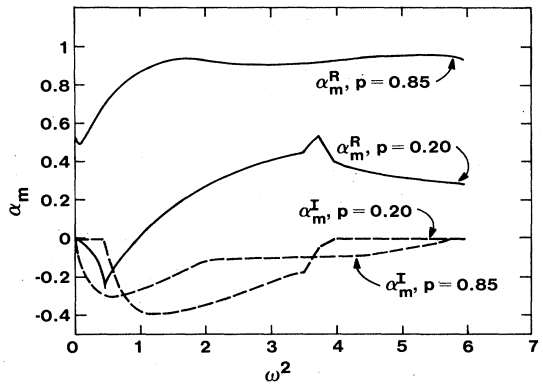

FIG. 8. Showing the real and imaginary parts of $\alpha_m(\alpha_m^R,\alpha_m^I)$ for $p=0.85$ and $p=0.20$ as a function of ω^2, where $\alpha/M=1$ and $\alpha=1$.

cies one must carefully search numerically for the other solution which is the correct one in this region. The less prominent cusplike feature in α_m^R and α_m^I ($p=0.20$) at $M\omega^2/\alpha=4.0$ is probably at least partially a numerical artifact, as it was difficult to solve the CPA equation at the right band edge for $p<p^*$.

V. CONCLUSIONS

The effective-medium-theory description of the vibrational behavior of nearest-neighbor central-force random elastic networks is now complete. Effective-medium theory describes both the elastic and finite frequency behavior of these networks with reasonable accuracy over the entire range of p, the fraction of bonds present. It is unusual for a simple effective-medium theory to be so accurate over such a broad range of system parameters (the other example that comes to mind is the simple mass defect[5]). A recent result[3] for longer-range central forces preserves this picture, showing again excellent agreement between EMT and numerical simulations for the elastic properties.

The EMT and the constraints argument *both* lead to a δ function at $\omega^2=0$ with weight $f(p)=1-p/p^*$. It is not entirely clear to us why these two very different approaches lead to the same result. It is important to understand this equivalence better as it serves to locate the transition at p^* by setting $f(p)=0$. Numerical simulations show that the EMT estimate of the number of zero frequency modes $f(p)$ is very accurate except very close to the transition.

Other workers have recently presented results for the density of states of depleted elastic networks.[13] These networks were different from ours in that sufficient microscopic forces were specified so that the networks were rigid for all $p>p_c$, the regular connectivity percolation threshold. The focus of that work appears to have been the effect of the fractal geometry of the percolation backbone on the density of states, in particular examining the crossover from a Debye-type spectrum to a fracton frequency regime as ω increased from zero. The exponent of the ω power law in the fracton regime was shown to depend on the fractal dimensionality of the percolating backbone. Effective-medium approximations have also been used to study such networks.[14]

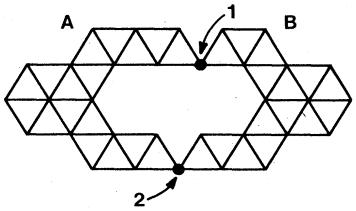

FIG. 9. Network units A and B are connected through pin joints 1 and 2. The connection fails to be rigid if *either* 1 or 2 is removed thus making the determination of the rigidity of the combined unit a nonlocal problem.

For our central-force random networks the situation is quite different. Since p^* is much larger than p_c for the triangular net, the geometry of the random networks is not fractal-like at the rigidity transition. However, the part of the network which can resist an external stress could very well be of fractal character. This rigid backbone is not easily identified, and thus its geometrical character remains unknown. That is why we have ignored the $\omega^2\rightarrow 0$ critical behavior in this paper in favor of those features of the spectrum more readily accessible to analysis, such as the overall shape of $g(\omega^2)$, the appearance of band gaps, and the fraction of zero-frequency modes. There are geometrical rules which have been formulated to identify sites which are not part of the rigid backbone at a given value of p, but these rules have been shown to be incomplete.[15] The difficulty of the problem is illustrated in Fig. 9, where unit A is rigidly connected to piece B through pin joints 1 and 2. The connection is only rigid however, if *both* 1 and 2 exist. If either joint is removed the entire connection fails. Thus the problem of determining whether A and B form a rigid unit is a nonlocal one and involves long-range effects as 1 and 2 can be separated by an arbitrarily large distance.

In summary, we have presented the first results for the finite-frequency response of a system undergoing a rigidity transition. We find that effect-medium theory for random central-force elastic networks is "almost exact" for the number of zero frequency modes and the elastic constants except near p^*, where only very small discrepancies with numerical simulations are observed. At finite frequency the effective-medium-theory description is very satisfactory and correctly shows the band gap opening up at $\omega^2=0$ when the networks' elastic properties are lost. It misses some important elements, however, such as the Lifshitz tails at the band edges and the structure due to small clusters in the dilute limit when $p\ll p_c$.

ACKNOWLEDGMENTS

It is a pleasure to thank S. D. Mahanti and J. B. Parkinson for several useful conversations and S. de Leeuw for reading the manuscript. The support of the National Science Foundation under Grant No. DMR 8317610 is gratefully acknowledged. One of us (E.J.G.) would like to thank Armstrong World Industries for time made available from other duties to work on this manuscript.

*Permanent address: Armstrong World Industries, Inc., Research and Development, P.O. Box 3511, Lancaster, PA 17604.

[1]S. Feng, M. F. Thorpe, and E. Garboczi, Phys. Rev. B **31**, 276 (1985).

[2]M. F. Thorpe, J. Non-Cryst. Solids **57**, 355 (1983).

[3]E. J. Garboczi and M. F. Thorpe, Phys. Rev. B **31**, 7276 (1985).

[4]S. Kirkpatrick, Rev. Mod. Phys. **45**, 574 (1973).

[5]For a general review of the coherent-potential approximation, see R. J. Elliott, J. A. Krumhansl, and P. L. Leath, Rev. Mod. Phys. **41**, 465 (1974).

[6]See, for example, N. W. Ashcroft and N. D. Mermin, *Solid State Physics* (Holt, Rinehart and Winston, Philadelphia, 1976) for the necessary formalism.

[7]R. J. Bell, in *Excitations in Disordered Systems,* edited by M. F. Thorpe (Plenum, New York, 1982); Methods Comput. Phys. **15**, 215 (1976); Rep. Prog. Phys. **35**, 1315 (1972).

[8]P. Dean, Rev. Mod. Phys. **44**, 127 (1972).

[9]The value of $p=0.50$ is less than even the result of Feng and Sen for $p^*=0.58$, so that there is no question that the elastic moduli are zero [S. Feng and P. N. Sen, Phys. Rev. Lett. **52**, 216 (1984)]. More recent results [M. A. Lemieux, P. Breton, and A.-M. S. Tremblay, J. Phys. (Paris) Lett. **46**, 1 (1985)] give $p^*=0.65$.

[10]R. Zallen, *The Physics of Amorphous Solids* (Wiley, New York, 1983).

[11]At low frequencies $g(\omega^2)=(2M/3\pi\sqrt{3}\alpha)(1-p^*)/(p-p^*)$ which gives the result $g(\omega^2)=(2M/3\pi\sqrt{3}\alpha)$ for the pure system as shown in Fig. 3, where $g(\omega^2=0)=0.1225$ with $\alpha/M=1$.

[12]I. M. Lifshitz, Adv. Phys. **13**, 483 (1964).

[13]I. Webman and G. Grest, Phys. Rev. B **31**, 1689 (1984).

[14]O. Entin-Wohlman, S. Alexander, R. Orbach, and K.-W. Yu, Phys. Rev. B **29**, 4588 (1984).

[15]E. J. Garboczi, Ph.D. thesis, Michigan State University, 1985.